Research Article | Vol. 15, No. 3 / 1 Mar 2024 / Biomedical Optics Express 1408

Biomedical Optics EXPRESS

Assessing cell viability with dynamic optical coherence microscopy

CHAO J. LIU,[1,*] JASON T. SMITH,[1] YUANBO WANG,[1] JONATHAN N. OUELLETTE,[1] JEREMY D. ROGERS,[2] JONATHAN D. OLINER,[1] MICHAEL SZULCZEWSKI,[1] ERIC WAIT,[1] WILLIAM BROWN,[3] ADAM WAX,[3] KEVIN W. ELICEIRI,[4] AND JOHN RAFTER[1]

[1] *Elephas Biosciences Corporation, 1 Erdman Place, Madison, WI 53717, USA*
[2] *Department of Ophthalmology and Visual Sciences, University of Wisconsin Madison, 2828 Marshall Ct, Madison, WI 53705, USA*
[3] *Lumedica Inc., 404 Hunt Street, Suite 510, Durham, NC 27701, USA*
[4] *Center for Quantitative Cell Imaging, 1675 Observatory Drive, Madison, WI 53706, USA*
[*] *cliu@elephas.com*

Abstract: Assessing cell viability is important in many fields of research. Current optical methods to assess cell viability typically involve fluorescent dyes, which are often less reliable and have poor permeability in primary tissues. Dynamic optical coherence microscopy (dOCM) is an emerging tool that provides label-free contrast reflecting changes in cellular metabolism. In this work, we compare the live contrast obtained from dOCM to viability dyes, and for the first time to our knowledge, demonstrate that dOCM can distinguish live cells from dead cells in murine syngeneic tumors. We further demonstrate a strong correlation between dOCM live contrast and optical redox ratio by metabolic imaging in primary mouse liver tissue. The dOCM technique opens a new avenue to apply label-free imaging to assess the effects of immuno-oncology agents, targeted therapies, chemotherapy, and cell therapies using live tumor tissues.

1. Introduction

Cell viability assays are important in many fields of research, including basic science, drug discovery and development, diagnostics, and toxicology. There are several methods for assessing cell viability, including monitoring changes in morphology, membrane permeability, and metabolic state [1]. However, each of these techniques has limitations, especially in intact live tissue samples. For example, morphological changes in cells are commonly assessed in monolayer assays and are typically difficult to quantify in three-dimensional (3D) tissues. The measurement of membrane permeability utilizes viability dyes that, while very effective in monolayer assays and flow cytometry applications, can be suboptimal in intact primary tissue due to their potential for low accuracy, non-specific labeling and poor diffusion into tissues [2,3]. High-throughput metabolic viability assays using tetrazolium salts are widely used; however, the accuracy of these assays require the optimization of cell number, tetrazolium salt concentration, and incubation time for different tissue types [4]. Moreover, assays utilizing labels require significant pretreatment time which can potentially perturb the sample and unduly influence the results. Therefore, there exists a need for more reliable and robust label-free approaches to assess cell viability in primary tissue assays which correlate to cessation of normal metabolic activity leading to cell death.

Intracellular organelles (such as mitochondria) are highly dynamic in live cells and their metabolic activities give rise to intracellular motions in live tissues. In contrast, dead tissues lack intracellular dynamics due to the absence of metabolic activities. Moreover, light scattered from particles is dependent on particle size and motion pattern [5] and therefore the dynamics in back scattered signal between live and dead tissues exhibit different signatures.

#509835 https://doi.org/10.1364/BOE.509835
Journal © 2024 Received 2 Nov 2023; revised 23 Jan 2024; accepted 23 Jan 2024; published 5 Feb 2024

Biomedical Optics EXPRESS

Optical coherence tomography (OCT) produces cross-sectional images of tissue structure at micrometer resolution [6]. OCT contrast originates from back scattering between tissue layers due to difference in refractive indices. Therefore, unlike conventional fluorescence microscopy, OCT provides label-free contrast. By raster scanning the OCT beam in the lateral plane, a 3D image volume of tissue structure can be obtained. OCT has gained popularity in various medical fields to visualize 3D tissue structures non-invasively, including ophthalmology and dermatology. The lateral resolution of traditional OCT is typically above 10 μm. Optical coherence microscopy (OCM), a variant of OCT, with high numerical aperture objective lenses can visualize cellular structures and achieve 2-3 μm lateral and ∼1 um axial resolution [7]. The increased optical resolution of OCM allows for detection of fluctuations that are less than the typical cell size, making OCM very sensitive to intracellular dynamics.

In recent years, the dynamic signals from OCT techniques have been used to visualize live cells in mouse tissue [8,9], human biopsy samples [10], and tumor organoids [11]. However, previous work has focused on the disruption of glycolysis in live tissues, and no comprehensive studies have been conducted to distinguish live cells from dead cells in the same tissue sample. Here we assess the ability of dynamic OCM (dOCM) contrast to distinguish live and dead cells in mouse syngeneic tumors and liver tissue. Dynamic OCM utilizes high-resolution OCM technology to capture a time series of tissue dynamics [8]. By analyzing the frequency components in the power spectrum of the time series, live cells with intracellular dynamics were highlighted by label-free dOCM contrast. Moreover, since OCM provides high-resolution depth-resolved images, dOCM can visualize live cells in 3D volumes.

2. Methods

2.1. Animals

Mouse tissues were obtained from the vivarium of Elephas Biosciences Corporation (Elephas, Madison, WI). For syngeneic tumors, CT26 cells were injected subcutaneously into both flanks of immunocompromised mice. Tumors were harvested at 200∼350 mm^3. Mouse livers were harvested immediately following euthanasia. All animal work was performed under Animal Care and Use Committee approved protocols which were in accordance with the Association for Assessment and Accreditation of Laboratory Animal Care guidelines.

2.2. Tissue process and culture

CT26 tumors were cut into $900 \times 900 \times 300$ μm^3 live tumor fragments (LTFs) with an automated tumor cutting instrument (Cybrid Edge, Elephas, Madison, WI). Phenol red-free RPMI (11835050, Fisher Scientific) supplemented with 10% FBS (10082147, Fisher Scientific), 10 mM HEPES (15630080, Gibco), 1 mM sodium pyruvate (S836, Sigma), 1X MEM non-essential amino acids (M7145, Sigma), 1X GlutaMax (35050061, Thermo Fisher), and 100 U/mL penicillin/streptomycin (15140122, Thermo Fisher) was used to culture the CT26 fragments (20% oxygen, 5% CO_2, 37 °C). In the absence of treatment, CT26 tumor fragments remained viable for at least 48 hours of culture (Supplement 1). For section 3.2, the fragments were cultured for 24 hours before experiments.

For mouse liver tissue, biopsy samples were collected with a 14-gauge biopsy needle (SuperCore 14 G, Argon Medical Devices, Wheeling, IL). Biopsies were segmented into 300 μm tissue "coins" with a Compresstome (VF-510-0Z, Precisionary Instruments, Natick, MA). The tissue was cultured overnight in phenol red-free Williams' E Medium (A12176, Thermo Fisher) inside a tri-gas incubator (80% oxygen, 5% CO_2, 37 °C) [12].

Biomedical Optics EXPRESS

2.3. OCM system

In this study, we used a Lumedica low-cost, high-resolution OCT system (OQ LabScope 3.0/SX, Lumedica, Durham, NC) [13,14] equipped with an objective lens (Olympus LCPLN20XIR, 0.45 NA). The center wavelength was at 880 nm with a bandwidth of ~180 nm. An additional motorized stage was controlled to move the sample. The imaging system was controlled by Elephas custom software which was also used for data acquisition. The Elephas software was built on Lumedica OQ Labscope software (coded in C#/.NET and C++). The intensity images were saved for further processing. To obtain the dOCM data, the time series of each cross section was first registered to the center frame. For each pixel in the time series of volumetric OCM intensity $I(x, y, z, t)$, fast Fourier transform was performed to obtain the power spectrum $P(x, y, z, f)$.

2.4. Multiphoton microscope

Fluorescence images were obtained on a modified inverted Bruker multiphoton microscope (MPM, Bruker, Billerica, MA) coupled to an inverted Zeiss Z1 microscope (Zeiss, Jena, Germany). Excitation and emission light were coupled through an air objective (Plan-Apochromat 20×/0.8, Zeiss). A titanium:sapphire laser (Chameleon, Coherent, Santa Clara, CA) was tuned to 740 nm to excite nicotinamide adenine dinucleotide (phosphate) (NAD(P)H) and 880 nm for flavin adenine dinucleotide (FAD) excitation. Bandpass filters, 460 ± 25 nm for NAD(P)H and 525 ± 25 nm for FAD, isolated the emitted fluorescence. Propidium iodide (1 µg/mL, P1304MP, Invitrogen) was added to the tissue culture 2 hours prior to imaging. The fluorescence intensity of propidium iodide was excited at 880 nm and emitted fluorescence was separated by a 625/30 nm bandpass filter. Fluorescence images were collected by GaAsP PMTs (10770, Hamamatsu, Japan).

2.5. Multimodal imaging and registration

The OCM system was mounted on top of the inverted multiphoton microscope. A stage-top incubator (Okolab, Pozzuoli, Italy) was used to maintain environmental conditions. Volumetric data were taken from both the upright OCM system and the inverted multiphoton microscope. Due to the limited penetrating depths, the tissues were flipped to ensure imaging data were from the same surface. Volumetric data were collected up to 100 µm in depth for both modalities and average intensity projections of the data were used for further analysis. The dOCM images were registered to the fluorescence images using non-rigid Demons registration algorithms. The NAD(P)H, FAD and propidium iodide images were co-registered. The optical redox ratio was defined as the fraction of NAD(P)H divided by the summed intensity of NAD(P)H and FAD [15].

2.6. Image analysis

Volumetric data of NAD(P)H and FAD were used to identify the centroids of individual cells using the surface rendering function in Imaris (v10.0, Oxford Instruments, Abingdon, UK). The centroid of each cell region was then used for Voronoi segmentation. For the receiver operating characteristics (ROC) analysis in Fig. 2 and the live percentage analysis in Fig. 3, the cell viability was determined by the intensity of propidium iodide within each Voronoi diagram as propidium iodide labels the nuclei of dead cells (see the example in Supplement 1). The ROC quantification was performed using customized MATLAB scripts. For the analysis in Fig. 3 and Fig. 5, the thresholds of live/dead status from dOCM live contrast and optical redox ratio of each experiment were obtained by the MATLAB function *multithresh* using Otsu's method.

Biomedical Optics EXPRESS

3. Results

3.1. Imaging cell viability using volumetric dOCM

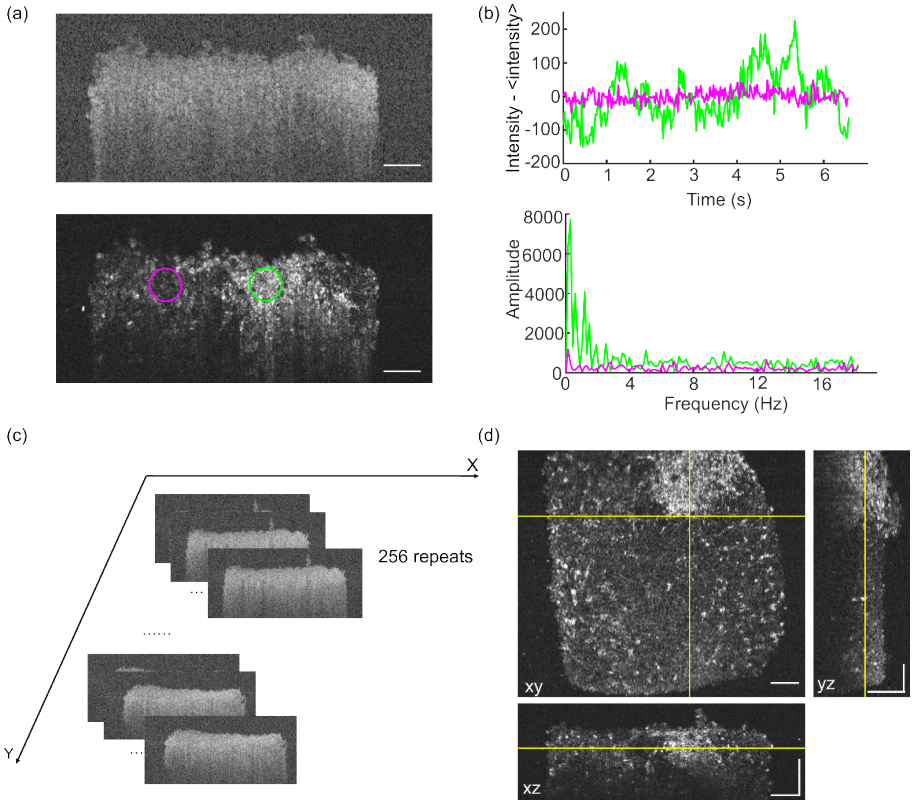

Fig. 1. Cell viability imaging protocol using dOCM. (a) OCM and dOCM images of the same cross-section from a CT26 tumor fragment. Green and magenta circles represent live and dead regions of interest as indicated in (b). (b) Upper panel: Intensity profiles of live (green) and dead (magenta) regions from the CT26 tumor fragment over 6.75 s. Lower panel: power spectral functions of the live (green) and dead (magenta) regions. The live frequency in this paper is defined as 0.1 Hz – 1 Hz. (c) Volumetric dOCM imaging protocol. 256 frames per cross section over 6.75 s are collected. (d) Single plane views of a CT26 tumor fragment. Yellow lines indicate the positions of adjacent xz and yz images. The upper right corner of the fragment contains numerous live cells, whereas the rest of the tissue contains scattered live cells. Scale bars: 100 µm.

We first developed the dOCM imaging protocol to access cell viability. Here we obtained 256 frames per cross section with each cross section containing 512 A-lines. The dynamic data per cross section was taken at an 80 kHz A-scan rate, which resulted in an effective B-scan rate of 38 Hz (20 ms delay time between each frame). Previous reports have demonstrated higher amplitude fluctuations in $P(x, y, z, f)$ in live tissues compared to dead tissues [8–10]. To enhance this contrast, we sought to determine the frequency spread of these fluctuations associated with live tissue. We obtained dOCM data from a CT26 tumor fragment, where both high and low levels of intracellular motions were observed (Fig. 1(b)). By averaging 50 pixels within regions of interest, higher levels of fluctuations in intensity were observed in the green region compared to the magenta region (Fig. 1(b), upper panel). In the frequency domain, higher fluctuations around

Biomedical Optics EXPRESS

1 Hz were observed in the green region, similar to previous reports [9–10]. We then defined the live signal as 0.16 Hz – 1 Hz in our system and obtained the dOCM image by averaging the amplitude within that frequency band (Fig. 1(a), lower panel).

For volumetric imaging, we first obtained the dynamic data from each cross section (B-M mode), where the tissue was moved by 4 μm increments laterally to image individual cross sections until the whole tissue was imaged (Fig. 1(c)). Volumetric cell viability data were obtained for the exemplary CT26 fragment (Fig. 1(d)). In the orthogonal views of the dOCM live contrast, numerous live cells with high intracellular motion can be seen in the upper right corner. Some scattered live cells can be seen in the other parts of the tissue, but most of the tissue exhibited reduced signal indicating that it was dead.

3.2. *Validating viability from dOCM by labeling dead cells with propidium iodide in syngeneic tumor tissue*

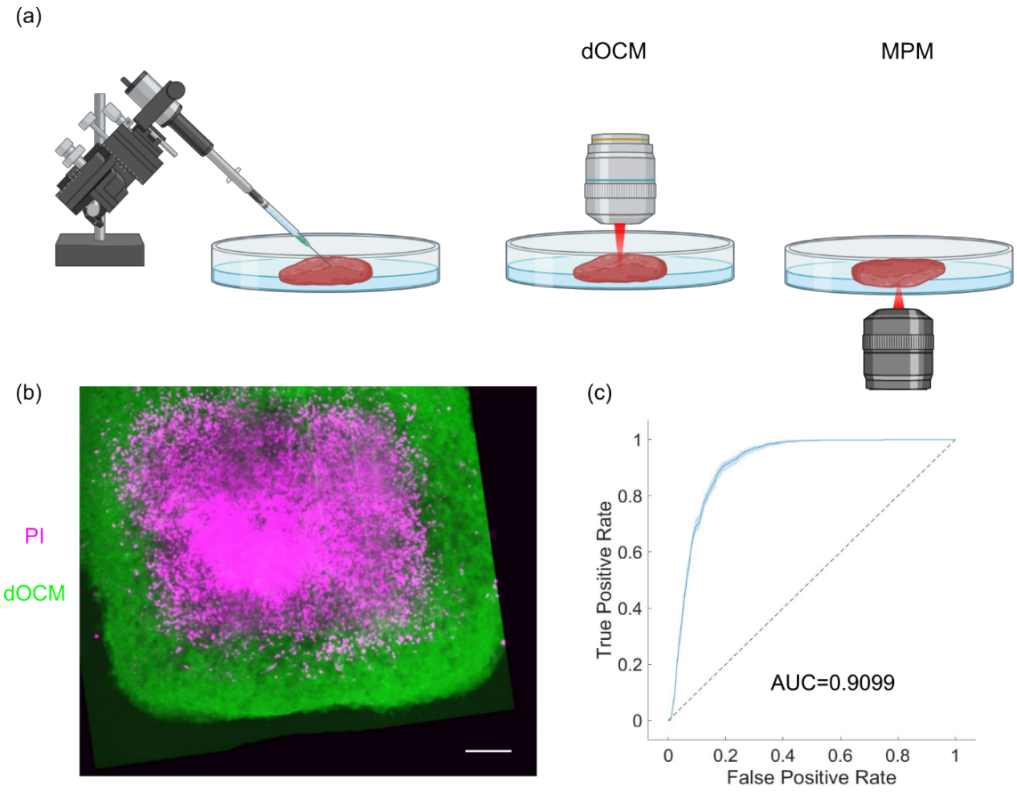

Fig. 2. Multimodal imaging of cell viability from dOCM and propidium iodide in CT26 syngeneic tumor tissue. (a) Multimodal imaging protocol. Local death in the center is introduced by microinjection of 3% H_2O_2 with a micromanipulator in CT26 fragments. Volumetric data of the fragment is collected by dOCM first and then by MPM after being flipped. (b) Registered propidium iodide (PI, magenta) and dOCM (green) images of the same fragment (also see Supplement 1). The images are both averaged intensity projection of 100 μm over depth. Scale bar: 100 μm. (c) Receiver Operating Characteristic (ROC) curve of dOCM contrast for live/dead status when PI is used as ground truth. The area under ROC is 0.9099.

To further verify the frequency band of live signals in our system and fully assess cell viability with dOCM contrast, a tissue sample with defined regions of live and dead cells was needed.

Biomedical Optics EXPRESS

We validated dOCM live contrast with propidium iodide, a gold standard for cell viability, often used in monolayer assays and syngeneic tissues. Here we performed experiments with a CT26 syngeneic tumor fragment, injecting it with H_2O_2 to induce cell death in the center but not in the periphery of the fragment (Fig. 2(a)).A microinjector (Nanofil 10 µL syringe and NF35BV-2 needle, WPI Instrument) driven by a micromanipulator (M3301R, WPI Instrument) was used to inject 500 nL of 3% H_2O_2 into the tissue. We then labeled the fragment with propidium iodide, a membrane-impermeable dye that is frequently used to identify dead cells. The fragment was first imaged by an upright OCT system, after which it was flipped, and the same region was imaged by an inverted multiphoton microscope (see Methods). Volumetric data were captured from both modalities (Fig. 2(a)) sequentially four hours after injection of H_2O_2.

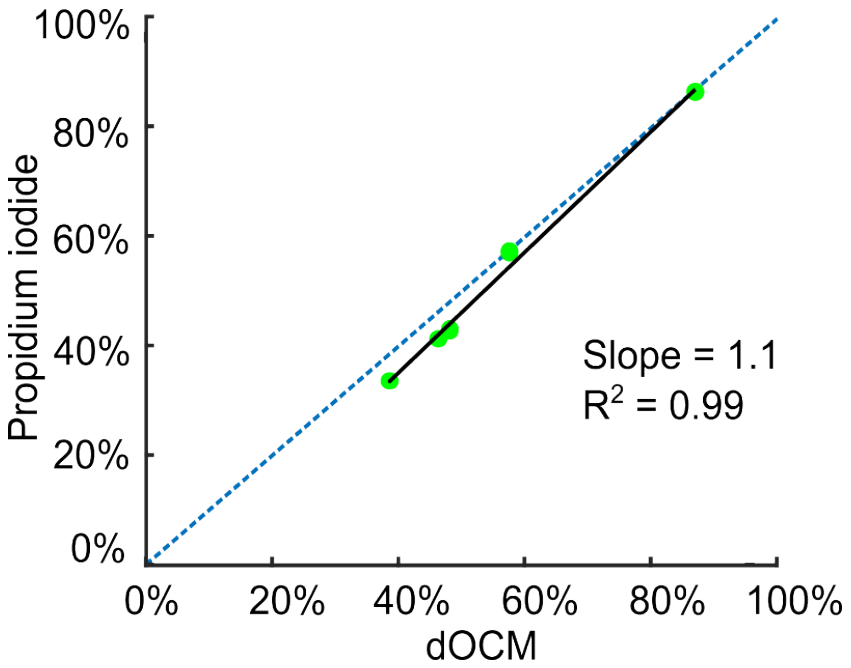

Fig. 3. The correlaion of cell viability derived from dOCM and propidium iodide. Each dot represents one experiment. The live percentage per fragment is calculated by dOCM (x-axis) and propidium iodide (y-axis), separately. The slope from linear fitting is 1.1 with a R^2 value of 0.99 over 5 experiments. The blue dashed line is the diagonal. The black line is the flitted curve.

Next, we registered the dOCM data to the propidium iodide fluorescence data. Propidium iodide staining indicating dead cells was only observed in the treated center of the CT26 fragment where H_2O_2 was injected. Here, the dOCM contrast was low compared to the live edges (Fig. 2(b), magenta: propidium iodide, green: dOCM live contrast; also see Supplemental Fig. 3 for separate gray scale images). We further quantified the receiver operating characteristics (ROC) of dOCM live contrast using propidium iodide as the ground truth. High accuracy was achieved for dOCM live contrast (Fig. 2(c), area under ROC = 0.9099).

An additional four CT26 fragments were injected with 3% H_2O_2. We quantified the live percentages of each fragment using propidium iodide and dOCM separately. The live/dead status of propidium iodide was determined by the propidium iodide intensity as depicted on the Voronoi segmented diagram (see Methods and Supplemental Fig. 2). Over five fragments, different live percentages were calculated. High correlation in viability between dOCM and propidium

Biomedical Optics EXPRESS

iodide was observed across the five data points (Fig. 3, dOCM vs. propidium iodide, slope = 1.1, R_2 = 0.99, p = 4.5e-4), suggesting that dOCM provides reliable contrast for cell viability.

3.3. *Correlating viability from dOCM with optical redox ratio via multiphoton microscopy in primary mouse liver*

To investigate the correlation between dOCM live contrast and optical redox ratio in primary tissue, we used fresh mouse liver tissue. Three different death mechanisms were studied: necrosis, apoptosis, and necroptosis (Fig. 4(a)). Injury to tissue due to cutting is known to induce necrosis [16]. Therefore, both live center and necrotic edges existed in the same tissue slice (Fig. 4(a), left panel). To induce apoptosis, we injected staurosporine (100 nL, 2 µM, Thermo Fisher), a non-selective inhibitor of protein kinases, (Fig. 4(a), middle panel). To induce necroptosis, we locally injected shikonin (100 nL, 6 µM, Tocris), a natural naphthoquinone pigment purified from *Lithospermum erythrorhizon* [17] (Fig. 4(a), right panel). We then sequentially collected dOCM and multiphoton-based intrinsic fluorescence data after overnight incubation. dOCM provided

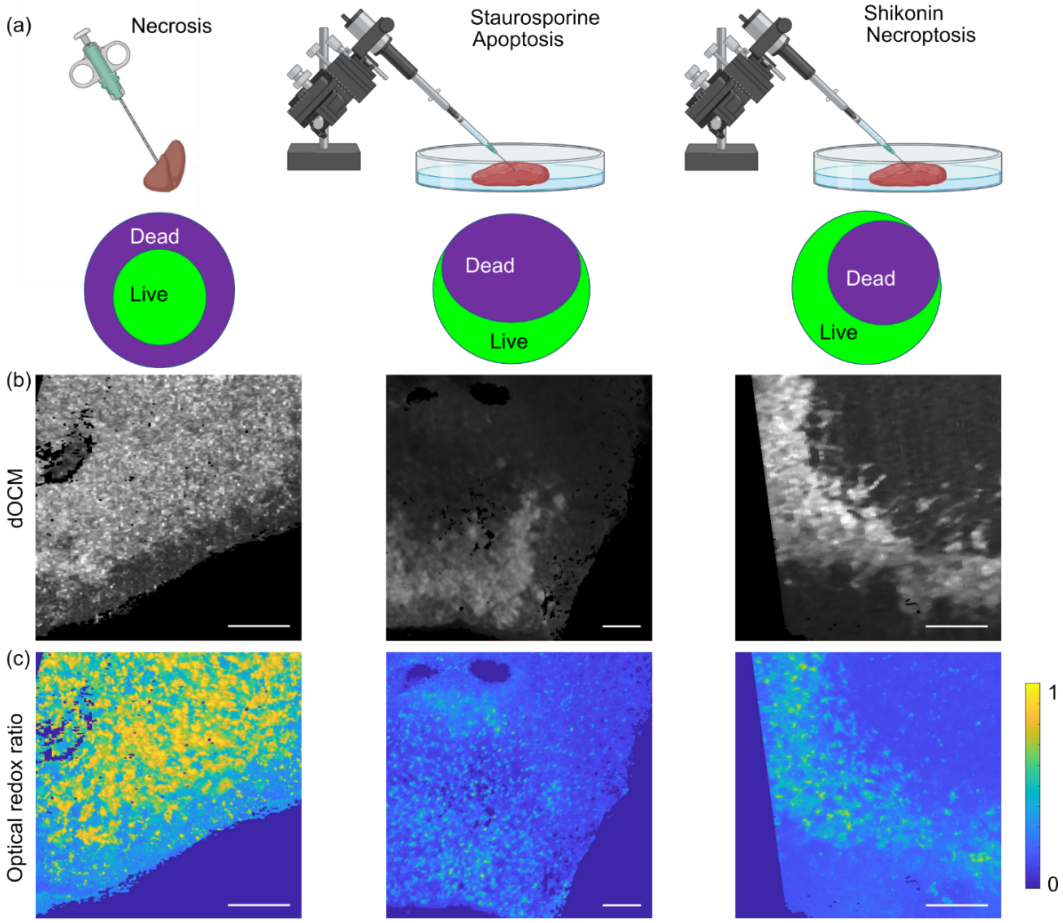

Fig. 4. Multimodal imaging of cell viability from dOCM and optical redox ratio via multiphoton microscopy in primary mouse liver tissue. Three different death mechanisms (a) are studied by mechanical damage (necrosis), local injection of staurosporine (apoptosis), and shikonin (necroptosis). dOCM (b) and optical redox ratio (c) images of the same mouse liver tissue. The optical redox ratio is indicated by the color bar in (c). Scale bars: 100 µm.

Biomedical Optics EXPRESS

separation between live and dead tissue across the three cell death mechanisms (Fig. 4(b)). We also performed intrinsic fluorescence based metabolic imaging from the same fragments and obtained the volumetric NAD(P)H and FAD intensity data. We analyzed the optical redox ratio and co-registered the two modalities (Fig. 4(a), see Methods). We observed higher optical redox ratios in the live cells compared to the dead region. Similarly, these live cells were highlighted by the dOCM live contrast (Fig. 4(b) and Fig. 4(c)). We observed heterogeneity in optical redox ratio in staurosporine treated primary mouse liver tissue consistent with staurosporine and chemotherapy treated primary cells [18,19]. To quantify this, we calculated the live percentage of each tissue fragment from the two modalities separately. By pooling results from all experiments, linear fitting was performed on the live percentages (Fig. 5, dOCM vs. optical redox ratio). The slope was 0.87 with $R_2 = 0.91$ ($p = 3.4e\text{-}3$), indicating a strong correlation between dOCM live contrast and optical redox ratio.

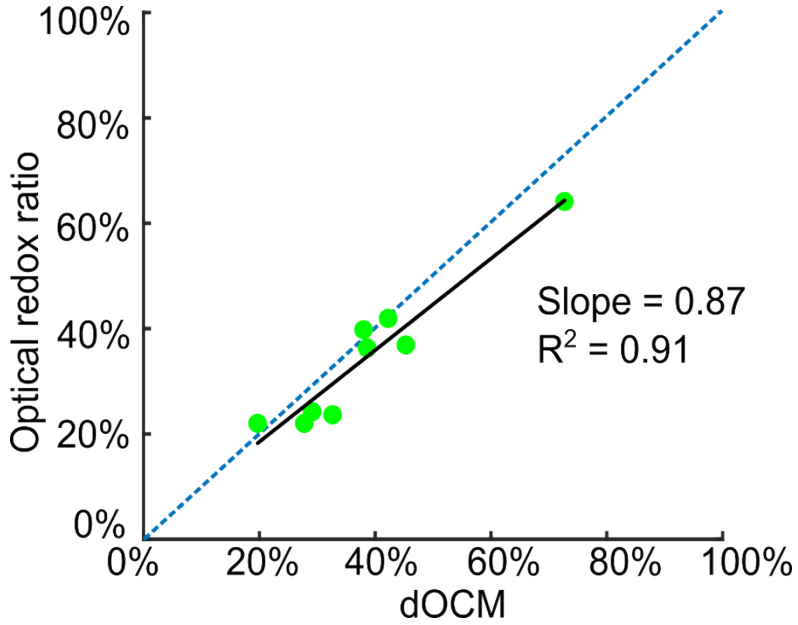

Fig. 5. The correlation of cell viability derived from dOCM and optical redox ratio. Each dot represents one experiment. The live percentage per fragment is calculated by dOCM (x-axis) and redox ratio (y-axis), separately. The slope from linear fitting is 0.87 with a R^2 value of 0.91 over 9 experiments including necrosis, apoptosis, and necroptosis (Fig. 4). The blue dashed line is the diagonal. The black line is the flitted curve.

4. Discussion

We presented dOCM as a reliable modality to assess cell viability. The dynamic signals from live cells can be obtained from a low-cost OCT system. On our instrument, live cells manifest fluctuations from 0.16 Hz to 1 Hz, which can be used to produce sensitive contrast from background via power spectral analysis. We validated the dOCM live contrast with the established cell death label propidium iodide and obtained high accuracy (Fig. 2 and Fig. 3). Cell death introduced by necrosis, apoptosis, and necroptosis was distinguished from live cells by dOCM live contrast (Fig. 4). Our data suggest that dOCM is a sensitive means of detecting live cells due to the active intracellular motions. In addition, by using intrinsic scattering dynamics

Biomedical Optics EXPRESS

of cellular structures, our work demonstrates that dOCM can be used in lieu of standard dye treatments to provide an unbiased approach to assess tissue viability.

In this work, we also showed a correlation between dOCM live contrast and optical redox ratio from NAD(P)H/FAD intensity (Fig. 4 and Fig. 5). Live cells showed higher levels of metabolism and intracellular motion. Apelian et al. showed dOCM is sensitive to metabolic energy production via glycolysis [8]. This is a potentially powerful avenue of exploration to discover and quantify metabolic differences across cell types that may be useful in identifying abnormal metabolic signatures in cells associated with pathologies such as cancer.

Robust quantification of cell viability using dOCM is an important future direction of our work. In this work, the dead regions lacked contrast whereas regions with sparse live cells showed cellular morphology (see Fig. 1(d)). Quantification of cell counts via morphological image analysis could be a robust way to advance dOCM technique for viability. Due to the limited resolution in our current system (~5 μm), we cannot resolve single cells in regions with dense cells. We are developing higher resolution dOCM (~1 μm isotropic resolution) to visualize single cells in densely populated regions with advanced image processing techniques.

In the present work, we did not investigate the dOCM frequency associated with membrane blebbing (i.e., dying cells). Membrane blebbing is one of most used criteria for distinguishing apoptosis from other physiological processes [20,21] and can potentially be detected by dOCM. We only provided the contrast mechanism between live cells and dead cells which lack intracellular motions (Fig. 2 and Fig. 4). One of our future directions is to develop an assay to analyze dOCM contrasts for dying cells and compare them with cell viability dyes such as Caspase-3/7 [22]. This correlation would be a promising indicator for programmed cell death mediated by immune cells and could help directly visualize T cell cytotoxic behavior, e.g., in ex vivo tumor tissue. The dOCM technology has the potential to provide rapid real-time profiling of LTFs with immuno-oncology agents, targeted therapies, chemotherapy, and cell therapies.

Acknowledgements. The study was funded by Elephas Biosciences Corporation. We thank the helpful discussion with Sean Caenepeel and the assistance from the Elephas team. The cartoons in Fig. 2 and Fig. 4 were generated from BioRender.

Disclosures. Elephas Biosciences Corporation has filed a provisional patent application 63/459,804 that encompasses aspects of the data described in this paper.

Data availability. Data underlying the results presented in this paper are not publicly available at this time but may be obtained from the authors upon reasonable request.

Supplemental document. See Supplement 1 for supporting content.

References

1. S. Johnson, V. Nguyen, and D. Coder, "Assessment of cell viability," *Curr. Protoc. Cytom., Chapter* **9** (2013).
2. C. Riccardi and I. Nicoletti, "Analysis of apoptosis by propidium iodide staining and flow cytometry," Nat. Protoc. **1**(3), 1458–1461 (2006).
3. M. Rosenberg, N. F. Azevedo, and A. Ivask, "Propidium iodide staining underestimates viability of adherent bacterial cells," Sci. Rep. **9**(1), 6483 (2019).
4. M. Ghasemi, T. Turnbull, S. Sebastian, *et al.*, "The MTT Assay: Utility, Limitations, Pitfalls, and Interpretation in Bulk and Single-Cell Analysis," Int. J. Mol. Sci. **22**(23), 12827 (2021).
5. J. Lee, W. Wu, J. Y. Jiang, *et al.*, "Dynamic light scattering optical coherence tomography," Opt. Express **20**(20), 22262–22277 (2012).
6. D. Huang, E. A. Swanson, C. P. Lin, *et al.*, "Optical coherence tomography," Science **254**(5035), 1178–1181 (1991).
7. J. A. Izatt, M. R. Hee, G. M. Owen, *et al.*, "Optical coherence microscopy in scattering media," Opt. Lett. **19**(8), 590–592 (1994).
8. C. Apelian, F. Harms, O. Thouvenin, *et al.*, "Dynamic full field optical coherence tomography: subcellular metabolic contrast revealed in tissues by interferometric signals temporal analysis," Biomed. Opt. Express **7**(4), 1511 (2016).
9. M. Münter, M. vom Endt, M. Pieper, *et al.*, "Dynamic contrast in scanning microscopic OCT," Opt. Lett. **45**(17), 4766–4769 (2020).
10. H. Leung, M. L. Wang, H. Osman, *et al.*, "Imaging intracellular motion with dynamic micro-optical coherence tomography," Biomed. Opt. Express **11**(5), 2768–2778 (2020).
11. I. A. El-Sadek, A. Miyazawa, L. T. Shen, *et al.*, "Optical coherence tomography-based tissue dynamics imaging for longitudinal and drug response evaluation of tumor spheroids," Biomed. Opt. Express **11**(11), 6231–6248 (2020).

Biomedical Optics EXPRESS

12. S. Kidambi, R. S. Yarmush, E. Novik, *et al.*, "Oxygen-mediated enhancement of primary hepatocyte metabolism, functional polarization, gene expression, and drug clearance," Proc. Natl. Acad. Sci. U.S.A. **106**(37), 15714–15719 (2009).
13. S. Kim, M. Crose, W. J. Eldridge, *et al.*, "Design and implementation of a low-cost, portable OCT system," Biomed. Opt. Express **9**(3), 1232–1243 (2018).
14. G. Song, K. K. Chu, S. Kim, *et al.*, "First Clinical Application of Low-Cost OCT," Trans. Vis. Sci. Tech. **8**(3), 61 (2019).
15. A. J. Walsh, K. P. Mueller, K. Tweed, *et al.*, "Classification of T-cell activation via autofluorescence lifetime imaging," Nat. Biomed. Eng. **5**(1), 77–88 (2020).
16. S. Elmore, "Apoptosis: A Review of Programmed Cell Death," Toxicol. Pathol. **35**(4), 495–516 (2007).
17. H. J. Kim, K. E. Hwang, D. S. Park, *et al.*, "Shikonin-induced necroptosis is enhanced by the inhibition of autophagy in non-small cell lung cancer cells," J. Transl. Med. **15**(1), 123 (2017).
18. A. J. Bower, J. E. Sorrells, J. Li, *et al.*, "Tracking metabolic dynamics of apoptosis with high-speed two-photon fluorescence lifetime imaging microscopy," Biomed. Opt. Express **10**(12), 6408–6421 (2019).
19. E. A. Shirshin, M. V. Shirmanova, A. V. Gayer, *et al.*, "Label-free sensing of cells with fluorescence lifetime imaging: The quest for metabolic heterogeneity," Proc. Natl. Acad. Sci. U.S.A. **119**(9), e2118241119 (2022).
20. A. H. Wyllie, J. F. R. Kerr, and A. R. Currie, "Cell death: the significance of apoptosis," Int. Rev. Cytol. **68**, 251–306 (1980).
21. M. L. Coleman, E. A. Sahai, M. Yeo, *et al.*, "Membrane blebbing during apoptosis results from caspase-mediated activation of ROCK I," Nat. Cell. Biol. **3**(4), 339–345 (2001).
22. M. Brentnall, L. Rodriguez-Menocal, R. L. De Guevara, *et al.*, "Caspase-9, caspase-3 and caspase-7 have distinct roles during intrinsic apoptosis," BMC Cell Biol. **14**(1), 32 (2013).